Theory-guided enhancement of CO_2 reduction to ethanol on Ag-Cu tandem catalysts via particle-size effects

Pranit Iyengar[†], Manuel Kolb[§], James R. Pankhurst[†], Federico Calle-Vallejo[§]*, Raffaella Buonsanti[†]*

[†] Laboratory of Nanochemistry for Energy (LNCE), Institute of Chemical Sciences and Engineering (ISIC), École Polytechnique Fédérale de Lausanne, CH-1950 Sion, Switzerland.

[§] Department of Materials Science and Chemical Physics & Institute of Theoretical and Computational Chemistry (IQTCUB), University of Barcelona, Martí i Franquès 1, 08028 Barcelona, Spain.

*Correspondence to: f.calle.vallejo@ub.edu, raffaella.buonsanti@epfl.ch

Abstract

In the CO_2 reduction reaction, the design of electrocatalysts that selectively promote alcohols over hydrocarbons (e.g., ethanol over ethylene) hinges on the understanding of the pathways and specific sites that forms alcohols. Herein, theoretical considerations guide state-of-the-art synthesis of well-defined catalysts to show that higher selectivity toward ethanol is achieved on Cu(110) edge sites compared to Cu(100) terraces. Specifically, we study the catalytic behavior of Cu nano-cubes (Cu_{cub}) of different sizes in the framework of tandem catalysis with CO-producing Ag nanospheres. We predict and experimentally find that the smaller Cu_{cub} possess higher selectivity for ethanol in view of their larger edge-to-faces ratio and of the fact that ethylene is produced at terraces while ethanol is selectively produced at step edges. These results call for synthetic developments toward Cu nanostructures exposing only edge sites, such as hollow cubic nanocages, to further increase ethanol selectivity. More generally, this study encourages the application of well-defined nano catalysts as a bridge between theory and experiments in electrocatalysis.

Introduction

The electrochemical CO_2 reduction reaction (CO_2RR) is a promising approach to address the rising atmospheric CO_2 levels by converting it into fuels and chemical feedstocks as forms of stored renewable energy.[1,2] Among single-metal surfaces, copper is the only catalyst capable of generating significant amounts of high-value C_{2+} hydrocarbons and oxygenates.[1,3,4] Compared to hydrocarbons, alcohols are generally obtained with considerably lower efficiencies.[1–6] The low alcohol-to-hydrocarbon ratios evidence our limited understanding of the catalyst structure sensitivity and possible reaction pathways toward alcohols.[7–18]

It is known that the early and late stages of CO_2 reduction (i.e., CO_2 to CO and CO to multi-carbon products, respectively) are efficiently catalyzed by different materials.[19,20] Therefore, tandem catalysis in which a CO-producing domain (e.g. Au, Ag, Zn, Fe porphyrins) is coupled to a Cu catalyst, has recently emerged as a promising strategy to promote C_{2+} products.[7,13,14,21–25] Yet, consensus on the mechanistic bifurcation point of the ethanol and ethylene pathways has not been reached and information on the structural and compositional sensitivities of ethanol formation are still largely missing.[7,14] Filling this knowledge gap is important to focus future experimental and computational efforts on rationally influencing the alcohol-to-hydrocarbon ratio during CO_2RR.

Recently, theory-coupled experimental studies have leveraged the facet-dependent selectivity of CO_2RR to provide insights into the mechanistic pathway toward ethanol formation.[7,25] Cu catalysts exposing (111) surfaces (i.e., Cu nano-octahedra) were shown to possess higher selectivity for ethanol than those exposing (100) surfaces (i.e., Cu nano-cubes) under local CO saturation induced by the coupling with Ag domains. DFT calculations revealed that $*CH_x$-*CO coupling is favored on the Cu(111) terraces under excess CO supply, which suggested this as the pathway leading to ethanol.[7,25] Theory also predicted an even greater enhancement on step edges. Meanwhile, the flat Cu(100) terraces (i.e., the predominant faces on Cu nano-cubes) continue to produce ethylene, thus mitigating the improvement expected.[7,25]

Herein, we provide a simplified semiempirical model which suggests that an increased edge-to-terrace ratio should foster the ethanol selectivity. To test this hypothesis, we combine Cu nano-cubes of different sizes with Ag nano-spheres in the framework of tandem catalysis. These well-defined Cu catalysts represent an ideal platform because the proportion of edges and corners versus the faces increases with decreasing size. [26–28]

Results and Discussion

To provide concrete experimental guidelines toward the design of ethanol-selective catalysts, we have simplified a previous model (for a full derivation and evaluation of the accuracy of our approximations, see the Supporting Information, SI, sections 2.1 – 2.3): [25]

$$\left(\frac{FE_{C_2H_5OH}}{FE_{C_2H_4}}\right)_{Tandem} \approx \left(\frac{FE_{C_2H_5OH}}{FE_{C_2H_4}}\right)_{Cu} + \frac{4d_{Cu-Cu}}{L} \cdot \frac{r^{edge}_{C_2H_5OH}}{r^{terrace}_{C_2H_4}} \quad (1)$$

where $FE_{C_2H_5OH}$ and $FE_{C_2H_4}$ are the respective Faradaic efficiencies for the tandem catalyst and the bare Cu catalyst, L is the length of the edge of the copper cubes, d_{Cu-Cu} is the interatomic distance in the copper lattice ($d_{Cu-Cu} = 0.2556\,nm$), and $r^{edge}_{C_2H_5OH}/r^{terrace}_{C_2H_4}$ is the ratio of the rates of ethanol production at the steps and ethylene at the (100) terraces given in Equation 2:

$$\frac{r^{edge}_{C_2H_5OH}}{r^{terrace}_{C_2H_4}} = e^{-0.5 \cdot \frac{\left(\Delta G^{\#}_{C_2H_5OH} - \Delta G^{\#}_{C_2H_4}\right)}{k_B T}} \quad (2)$$

where k_B is the Boltzmann constant, T is the temperature in *K*, and $\Delta G_i^{\#}$ are the largest reaction barriers toward the specific products. We chose 0.5 as a typical value for the symmetry factor.[29] This is usually a good assumption, except when analyzing the actual electrochemical step where a pathway bifurcation occurs,[30,31] which is not the case here.

Since ethanol is thought to be mainly produced at steps and ethylene at (100) terraces,[1–3,32] the model predicts that the size of the cubes will directly impact the ethanol yield of the reaction. Smaller cubes (i.e., those in which the term *L* is smaller) should enhance the performance of the tandem catalyst, provided that the exponential term is approximately constant within the range of sizes inspected. This is likely the case for nanoparticles above 2-3 nm, which have converged adsorption energies, as shown in previous studies.[33–35] Based on this prediction, we designed suitable CO_2RR experiments to test it.

Cu nanocubes (Cu_{cub}) with average sizes (i.e., edge length) of 25, 37 and 52 nm were synthesized by fine-tuning the reaction between CuBr and trioctylphosphine oxide in oleylamine (details provided in the Experimental Section). The Cu_{cub} were combined with Ag nanospheres (Ag_{sph}) to form the Cu_{cub}-Ag tandem catalysts. The Cu:Ag calculated surface area ratio was maintained fixed at 1:2 across the Cu_{cub} sizes. This ratio was selected based on a

screening reported previously, which indicated it to be optimal for the CO consumption by the middle-sized Cu_{cub}.[25] Transmission electron microscopy (TEM) was used to characterize the morphology of the catalysts before and after CO_2RR. The as-prepared catalysts consist of homogeneously mixed and well dispersed size-controlled Cu_{cub} and Ag_{sph} (**Figure 1 A-D**). After 15 min of electrolysis, the Cu_{cub} preserve their morphologies, while the Ag_{sph} form a network intimately surrounding the Cu NCs (**Figure 1 E-G**), in agreement with previous studies.[26,36,37] These structures remain unchanged after 1 h of operation. The X-ray diffraction (XRD) pattern (**Figure 1 H**) evidences the characteristic features of the Cu_{cub}, with preferential orientation along the (100) plane. The peak corresponding to the Ag_{sph} is less intense and broader due to the considerably smaller size of the crystallites. Consistent with our previous work, similar X-ray photoelectron spectroscopy (XPS) data were obtained after CO_2RR (SI Section 1.6 and **Figure S1**). While it cannot be completely ruled out, we expect any potential interfacial alloying to be similar for all the Cu_{cub}-Ag catalysts and, thus, not to play a major role in the following discussion of the catalytic trends.

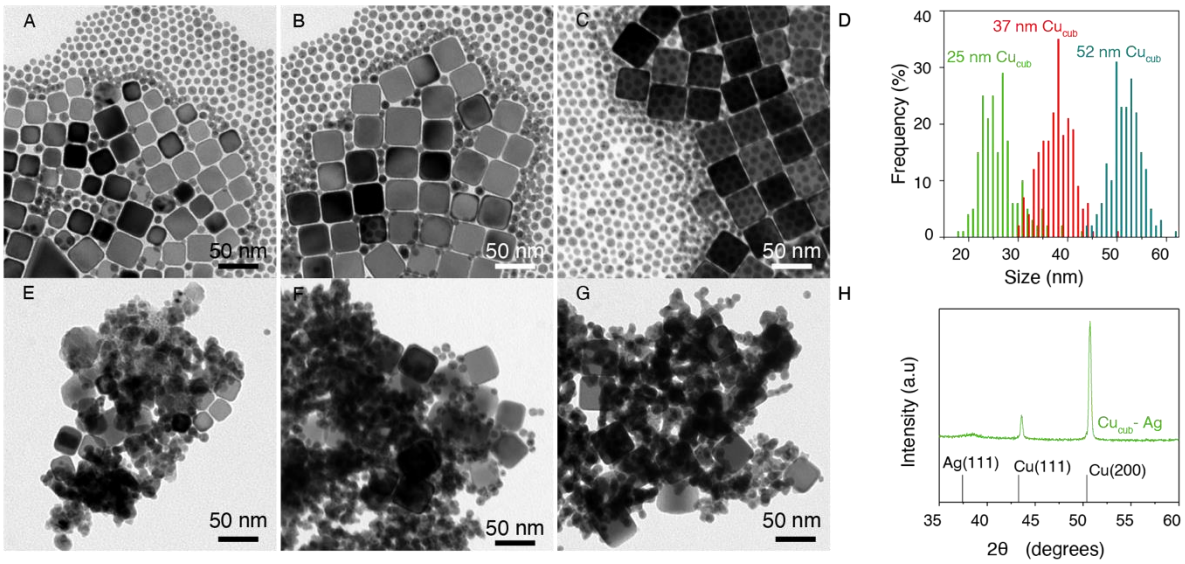

Figure 1. TEM images of as-prepared Cu_{cub}-Ag using 9 nm Ag_{sph} with (A) 25 nm, (B) 37 nm, and (C) 52 nm Cu_{cub}, respectively; (D) Size histograms of the Cu NCs; (E-G) TEM images of the corresponding catalysts after 15 min of electrolysis in 0.1 M $KHCO_3$ at −1.3 V_{RHE}; (H) Representative XRD of the Cu_{cub}–Ag catalyst drop-cast onto a Si wafer.

The performance of the Cu_{cub}-Ag catalysts for CO_2RR was evaluated in a typical H-type liquid cell with the catalysts drop-cast on flat glassy-carbon electrodes. All the samples underwent solvent washing to remove ligands from the surface, as described in the SI, Section 1.4. Potentials were applied between −1.1 V_{RHE} and −1.3 V_{RHE} (RHE: reversible hydrogen

electrode); outside of this range, the Cu NCs alone yielded hydrogen as the major product, which is consistent with previous studies.[26,27,36,38]

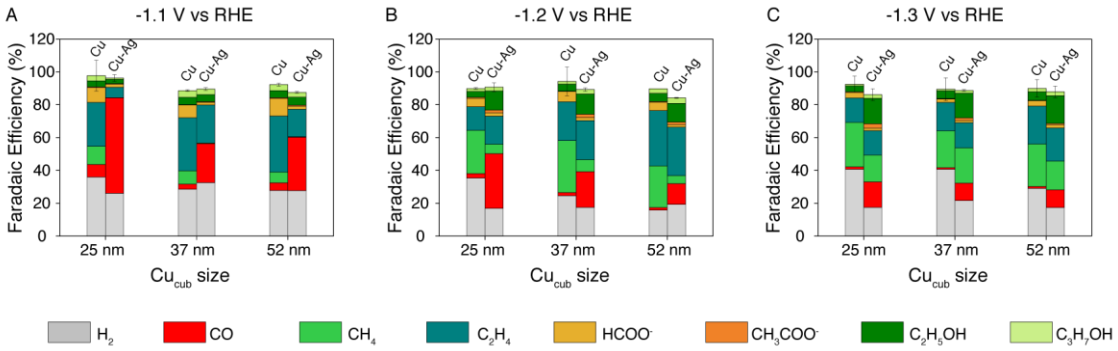

Figure 2. FEs for the Cu_{cub}-Ag catalysts prepared with Cu_{cub} of different sizes at potentials of (A) -1.1 V, (B) -1.2 V and (C) -1.3 V vs RHE at Cu mass loading of 15 μg/cm^2. The FEs for the bare Cu_{cub} of the same sizes and loading are also reported. The CO_2RR measurements were carried out using glassy-carbon electrodes as the substrate and CO_2-saturated 0.1 M $KHCO_3$ electrolyte. The reported values are the average of three independent experiments.

Figure 2 reports the Faradaic efficiencies (FEs) toward gas and liquid products for the Cu_{cub}–Ag catalysts prepared with the three different sizes of Cu_{cub}, compared to the bare Cu_{cub} counterparts, at variable potentials. It is observed that the addition of Ag generally suppresses the hydrogen evolution reaction (HER), which is related to the competition between *H and *CO for active sites on Cu.[23,39] This effect is particularly evident at -1.2 V_{RHE} for the 25 and 37 nm Cu_{cub}, and for all three sizes of Cu_{cub} at -1.3 V_{RHE}.

The FE_{CO} increases in the tandem catalysts, concomitant with the addition of the CO-producing Ag spheres. This increase is particularly drastic at -1.1 V_{RHE}, where the activity of the Cu_{cub} is lower, in agreement with previous studies.[22,21] Comparing Cu_{cub} sizes for a given potential, the FE_{CO} decreases with increasing Cu_{cub} size on the Cu_{cub}–Ag catalysts. This finding indicates that larger Cu_{cub} are better at consuming the locally produced CO and subsequently reducing it to other CO_2RR products.

The FE_{CH4} is suppressed on the Cu_{cub}-Ag catalysts across the entire potential and size range. This trend is most evident at −1.2 V_{RHE}; for example, FE_{CH4} drops from 26% in the bare 25 nm Cu_{cub} to 5% in the corresponding Cu_{cub}-Ag catalyst. At -1.1 V_{RHE}, where not much CH_4 is produced on the bare Cu_{cub}, this product completely disappears in the Cu_{cub}-Ag catalysts. At -1.3 V_{RHE}, a decrease is still observed (e.g., comparing the bare 25 nm Cu_{cub} catalyst to the corresponding Cu_{cub}-Ag catalyst), although it is relatively small. This finding might be

connected to the fact that more cathodic potentials promote C_1 pathways over C-C coupling to C_{2+} products.[17,33]

Moving to the C_{2+} products, the FE_{C2H4} for the Cu_{cub}–Ag at -1.1 V_{RHE} is reduced compared to the bare Cu_{cub}, which is related to the increased CO production due to high Ag activity at this lower potential. At -1.2 and -1.3 V_{RHE}, the FE_{C2H4} for all the Cu_{cub}-Ag catalysts does not change appreciably with the addition of Ag compared to the bare Cu_{cub}. This finding suggests that the C_2H_4-selective sites have a sufficiently high coverage of *CO even without Ag, such that they are not drastically affected by the additional local supply of CO.[7,40] Across the different Cu_{cub} sizes, the FE_{C2H4} in the Cu_{cub}–Ag catalysts increases as the Cu_{cub} sizes increases. The FE_{C2H4} changes from 17 to 30% at -1.2 V_{RHE} and from 14 to 20% at -1.3 V_{RHE} going from a length of 25 to 52 nm in the Cu_{cub}–Ag catalysts.

The FE_{C2H5OH} does not change appreciably with size at -1.1 V_{RHE} without Ag, however it does increase at -1.2 and -1.3 V_{RHE} for all the Cu_{cub}-Ag catalysts. At -1.2 V_{RHE} it changes from 3-5% on the Cu_{cub} catalysts to 11-12% on the Cu_{cub}-Ag catalysts, and at -1.3 V_{RHE} from 3-5% on the Cu_{cub} catalysts to 15-17% on the Cu_{cub}-Ag catalysts. No specific size-dependent behavior is observed. Apart from the suppression of formate on the Cu_{cub}-Ag catalysts with respect to Cu_{cub}, no other major changes were observed in the detected liquid products.

As the efficiency of Cu_{cub} to convert CO from Ag via tandem catalysis improves at the more cathodic potentials of -1.2 and -1.3 V_{RHE}, these potentials will hence be the focus of the following discussions. To delineate subtleties across the Cu_{cub} sizes and identify comparative trends among the CO_2RR products, **Figure 3** shows the FE ratios of C_2/C_1 (**Figure 3A**) and C_2H_5OH/C_2H_4 (**Figure 3B**) for the Cu_{cub}-Ag compared with the bare Cu_{cub} catalysts.

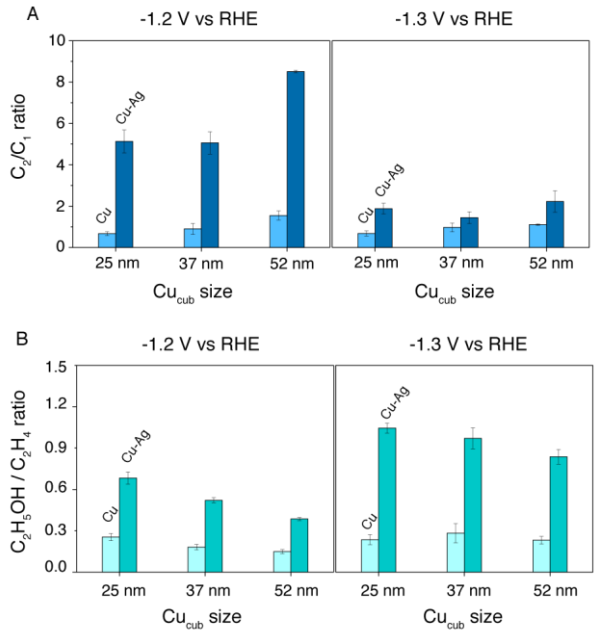

Figure 3. (A) FE_{C2}/FE_{C1} and (B) FE_{C2H5OH}/FE_{C2H4} of the Cu_{cub}-Ag compared with bare Cu_{cub} for variable Cu_{cub} size at -1.2 and -1.3 V_{RHE} with Cu mass loading of 15 μg/cm^2. The CO_2RR measurements were carried out using glassy-carbon electrodes as the substrate and CO_2-saturated 0.1 M $KHCO_3$ electrolyte. The reported values are the average of three independent experiments.

Firstly, the C_2/C_1 FE ratios are higher for all the Cu_{cub}–Ag catalysts compared to the corresponding bare Cu_{cub} catalyst in agreement with previous studies on tandem schemes.[7,13,14,21–24] At -1.2 V_{RHE} the C_2/C_1 FE ratio increases alongside the size of Cu_{cub} for the Cu_{cub}–Ag catalysts. Specifically, it changes from 5.1 to 8 going from 25 to 52 nm in the Cu domain size for the Cu_{cub}–Ag catalysts. At -1.3 V_{RHE}, the C_2/C_1 FE ratio for the three Cu_{cub}–Ag catalysts remains within standard deviation of each other.

Among the C_2 products, the C_2H_5OH/C_2H_4 FE ratio increases for all the Cu_{cub}–Ag catalysts compared to the corresponding bare Cu_{cub} catalyst. As for the size-dependence, the C_2H_5OH/C_2H_4 FE ratio decreases as the Cu_{cub} size increases. In particular, the C_2H_5OH /C_2H_4 FE ratio decreases from 0.7 to 0.4 at -1.2 V_{RHE} as the Cu_{cub} size increases from 25 to 52 nm in the Cu_{cub}–Ag catalysts. The trend is consistent even at -1.3 V_{RHE}, but it seems more subtle due to diminishing differences between the bare Cu_{cub} themselves at this potential.

While the FEs provide an idea of general trends in the product distribution, the partial current densities illustrate differences in the intrinsic activity changes toward specific products. **Figure 4** reports the current densities normalized by the electrochemically active surface area (J_{ECSA}) relative to the major CO_2RR products for all the samples at -1.2 and -1.3 V_{RHE}.

The $J_{ECSA}(CH_4)$ decreases for all the Cu_{cub}-Ag catalysts compared to the bare Cu_{cub} at -1.2 V_{RHE} (**Figure 4A**), indicating that the production rate of CH_4 is suppressed. At -1.3 V_{RHE}, the large driving force toward CH_4 minimizes the differences between the Cu_{cub}-Ag and the bare Cu_{cub}. Therefore, it decreases less dramatically for the smaller Cu_{cub} size and remains roughly the same for the bigger Cu_{cub}. Overall, not much change is observed in the $J_{ECSA}(C_2H_4)$ when comparing the Cu_{cub}-Ag catalysts to the bare Cu_{cub} (**Figure 4B**). Finally, $J_{ECSA}(C_2H_5OH)$ dramatically increases with the addition of Ag to all the Cu_{cub} at both potentials. Regarding the size dependence, at -1.2 V_{RHE} it decreases slightly when going from 25 to 52 nm for the Cu_{cub}–Ag catalysts. At -1.3 V_{RHE} the decrease with increasing Cu_{cub} size is more evident, going from 1.6 mA/cm^2 for the 25 nm Cu_{cub}–Ag to 0.6 mA/cm^2 for the 52 nm Cu_{cub}–Ag.

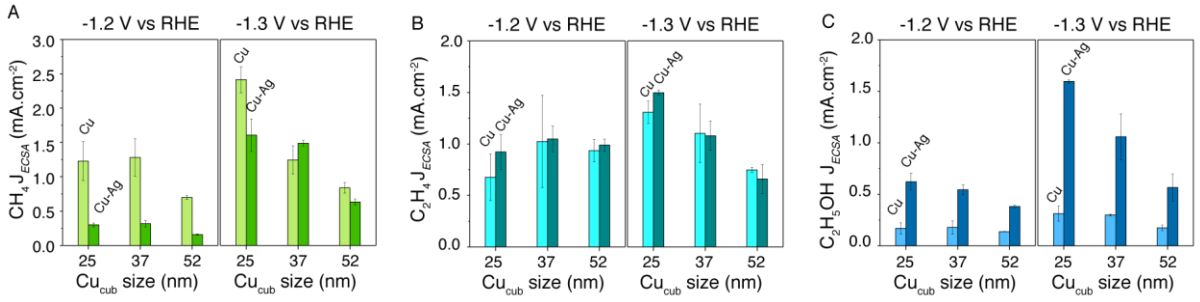

Figure 4 ECSA-normalized partial current densities (J_{ECSA}) at -1.2 and -1.3 V_{RHE} for (A) CH_4, (B) C_2H_4 and (C) C_2H_5OH of the Cu_{cub}-Ag catalysts, with a Cu mass loading of 15 μg/cm^2.

To further highlight the relative changes in the Cu_{cub}-Ag compared to the bare Cu_{cub} catalysts, the enhancement factors (i.e. the ratio of J_{ECSA} of the Cu–Ag catalyst to the J_{ECSA} of the corresponding bare Cu NC catalyst) are reported in **Figure 5** for CH_4, C_2H_4 and C_2H_5OH**.** These graphs show that the production of CH_4 is generally low, C_2H_4 production remains nearly unchanged and C_2H_5OH production is enhanced for all the Cu_{cub}-Ag ensembles. In particular, C_2H_5OH production exhibits a more pronounced size dependence which is most prominent at -1.3 V_{RHE}. At this potential, the production rate of C_2H_5OH increases up to 5 times for the Cu_{cub}-Ag catalyst with 25 nm Cu_{cub} compared to the corresponding Cu_{cub} and then decreases with increasing Cu_{cub} size.

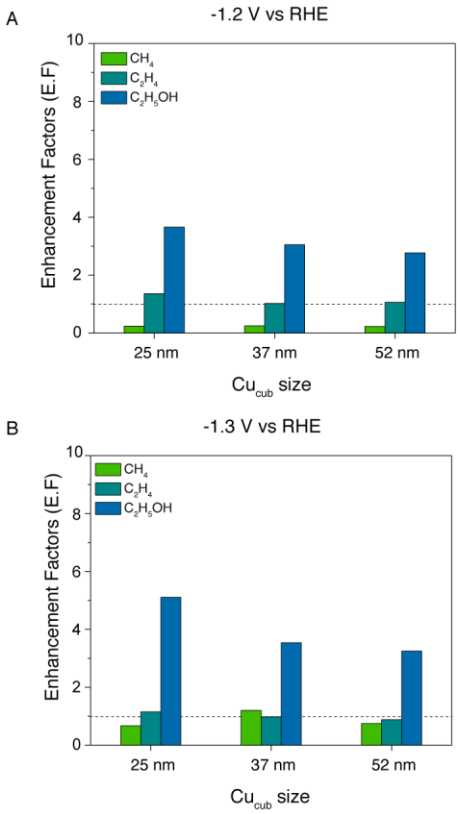

Figure 5. CH_4, C_2H_4 and C_2H_5OH enhancement factors for the Cu_{cub}–Ag catalysts at (A) -1.2 V_{RHE} and (B) -1.3 V_{RHE}. Enhancement factors are calculated as the ratio of J_{ECSA} of the Cu–Ag catalyst to the J_{ECSA} of the corresponding bare Cu NC catalyst.

Taking all of the above data into account, a complete picture emerges. It should be considered that as the Cu_{Cub} size decreases, the area ratio of (110) edges to (100) faces increases. As shown in **Table 1**, such ratio can be estimated to be 1.97, 2.76 and 4.09% for the 52, 37 and 25 nm Cu_{cub}, respectively (details in the SI, section 2.2). The higher proportion of (100) facets for the same overall surface area in the larger Cu_{cub} explains why the FE_{C2H4} in **Figure 2** increases with size and, consequently, the C_2H_5OH/C_2H_4 FE ratio in **Figure 3** decreases with size in the Cu_{cub}–Ag catalysts. The similar $J_{ECSA}(C_2H_4)$ between the Cu_{cub} and Cu_{cub}–Ag can be rationalized by the C_2H_4-selective sites having a relatively high coverage of *CO even in the absence of tandem catalysis, and hence were not significantly affected.[7,40]

The size-dependence of $J_{ECSA}(C_2H_5OH)$ clearly evidences that the intrinsic activity of the smaller Cu_{cub} toward C_2H_5OH is enhanced in the presence of the local supply of CO from the Ag_{sph}. The observation that the increase in J_{ECSA} (C_2H_5OH) is accompanied by a decrease of $J_{ECSA}(CH_4)$ is consistent with C_2H_5OH and CH_4 sharing similar active sites and/or with C_2H_5OH forming via *CO-*CH_x coupling. This phenomenon is also reflected in the suppression of FE_{CH4} accompanied by the enhancement of FE_{C2H5OH}, as discussed in **Figure 2**.

Finally, the enhancement factor of C_2H_5OH peaking at the 25 nm Cu_{cub} size and decreasing with increasing Cu_{cub} size, are indicative of a smaller proportion of C_2H_5OH-selective sites taking advantage of the local CO supply on the larger Cu_{cub}. The higher ratio of edge-to-terrace sites in the small Cu_{cub} justifies this behavior.

To close this section, we have applied Equation 1 to calculate the ratio of the reaction rates (r) of ethanol and ethylene in the Cu_{cub}-Ag catalysts relative to the bare Cu_{cub} of the same size. To achieve improved numerical stability, we calculate the reaction-rate averages $\left(r^{edge}_{C_2H_5OH}/r^{terrace}_{C_2H_4}\right)^{avg}$ using all our size-dependent experimental data as follows:

$$\left(\frac{r^{edge}_{C_2H_5OH}}{r^{terrace}_{C_2H_4}}\right)^{avg} = \frac{\Delta\left(\frac{FE_{C_2H_5OH}}{FE_{C_2H_4}}\right)_{Tandem} - \Delta\left(\frac{FE_{C_2H_5OH}}{FE_{C_2H_4}}\right)_{Cu}}{4d\left(\frac{1}{L_2}-\frac{1}{L_1}\right)} \quad (3)$$

where $\Delta\left(FE_{C_2H_5OH}/FE_{C_2H_4}\right)_{Tandem}$ is the difference between $\left(FE_{C_2H_5OH}/FE_{C_2H_4}\right)_{Tandem}$ for sizes L_2 and L_1 for the Ag-Cu tandem catalysts, $\left(FE_{C_2H_5OH}/FE_{C_2H_4}\right)_{Cu}$ is the corresponding difference for pure copper, and L_1 and L_2 are the respective edge lengths of the cubes (25, 37 or 52 nm).

Table 1 reports $\left(r^{edge}_{C_2H_5OH}/r^{terrace}_{C_2H_4}\right)^{avg}$ for the two different applied potentials and all possible combinations of L_2 vs L_1, based on the data tabulated in the SI, section 2.4. The values for -1.2 V_{RHE} are centered around 9.70, indicating that the step edges are significantly more active for ethanol production than the terraces are for ethylene production by about one order of magnitude, with a standard deviation of 3.21. At -1.3 V_{RHE} the average is 9.91 with a standard deviation of 0.65. These results indicate that the cube edges are more active for ethanol production than the terraces are for ethylene production by about one order of magnitude. At the same time, the number of active sites for ethanol production is significantly lower compared to those for ethylene production by about a factor of 25 (Table S4). Consequently, despite the tenfold higher activity of these sites, the overall reaction rate is lower, which is reflected in the C_2H_5OH/C_2H_4 ratios being close to 1 or lower in Figure 3B.

Table 1. Average ratios of the reaction rates for ethanol production at edges and ethylene production at (100) terraces for different sizes at -1.2 and -1.3 V_{RHE}.

L_1, L_2	$\left(\frac{r^{edge}_{C_2H_5OH}}{r^{terrace}_{C_2H_4}}\right)^{avg}_{-1.2\ V_{RHE}}$	$\left(\frac{r^{edge}_{C_2H_5OH}}{r^{terrace}_{C_2H_4}}\right)^{avg}_{-1.3\ V_{RHE}}$
$37\ nm, 25\ nm$	6.79	9.32
$52\ nm, 37\ nm$	13.14	10.61
$52\ nm, 25\ nm$	9.18	9.80
mean	9.70	9.91
standard deviation	3.21	0.65

We also examined the predicted barrier differences by means of Equation 2. We calculate $\Delta G^{\#}_{C_2H_5OH} - \Delta G^{\#}_{C_2H_4}$ to be approximately -0.12 eV at both -1.2 and -1.3 V_{RHE}. These values indicate that the barriers for ethanol production are lower than those of ethylene production. Moreover, the barriers calculated previously for *CO-*CO coupling to produce ethylene on Cu(100) are in the range of 1.19-1.22 eV at 0 V_{RHE},[9,15] with a corresponding symmetry factor of ~2/3.[9] Consequently, $\Delta G^{\#}_{C_2H_4}$ is ~0.39 and 0.32 eV at -1.2 and -1.3 V_{RHE}, respectively. Using these results, $\Delta G^{\#}_{C_2H_5OH}$ can be estimated to be ~0.27 and ~0.20 eV at -1.2 and at -1.3 V_{RHE}, respectively. These barriers are well below the limit for fast kinetics at room temperature ($\Delta G^{\#} < 0.75\ eV$) set from transition-state theory.[1] Therefore, the semiempirical model suggests fairly swift kinetics for CO_2RR to ethylene and ethanol in the potential range of -1.2 to -1.3 V_{RHE}, with lower barriers for ethanol. All this demonstrates that models based on semiempirical equations, such as Equations 1 and 2, can be used to give fair estimations of potential-dependent barriers, which are rarely found in the literature in view of their complicated computational assessment.[1]

Conclusions

Theory becomes more valuable in electrocatalysis when it is not just corroborative but also predictive and experimentally validated. In this study, we provide a simple model to anticipate the size-dependent behavior of Cu cubes in the framework of tandem catalysis. We verify the validity of its predictions by testing Cu cubes of different sizes. Indeed, we find that increasing the edge contribution to the surface area of Cu cubes enhances the ethanol/ethylene ratio. The model is also used to predict average potential-dependent electrochemical barriers for ethanol formation, which are rather difficult to calculate with DFT.

Overall, this study aims at inspiring the future theory-driven design of catalysts, specifically of Cu catalysts for CO_2 reduction with improved selectivity and activity toward ethanol. For example, increasing efforts to achieve superior control over the exposed defect/step facets of Cu nanoparticles or toward the synthesis of hollow Cu cages exposing mostly undercoordinated sites should be highly sought after.

Acknowledgments

This work was financially supported by Gaznat S.A. JRP acknowledges the H2020 Marie Curie Individual Fellowship grant SURFCAT with agreement number 837378. The theoretical effort was supported by Spanish MICIUN's RTI2018-095460-B-I00, Ramón y Cajal RYC-2015-18996, and María de Maeztu MDM-2017-0767 grants, and partly by Generalitat de Catalunya via 2017SGR13. MJK and FCV are thankful to Red Española de Supercomputación (RES) for super-computing time at SCAYLE (projects QS-2019-3-0018, QS-2019-2-0023, and QCM-2019-1-0034). The use of supercomputing facilities at SURFsara was sponsored by NWO Physical Sciences.

References

(1) Nitopi, S.; Bertheussen, E.; Scott, S. B.; Liu, X.; Engstfeld, A. K.; Horch, S.; Seger, B.; Stephens, I. E. L.; Chan, K.; Hahn, C.; Nørskov, J. K.; Jaramillo, T. F.; Chorkendorff, I. Progress and Perspectives of Electrochemical CO_2 Reduction on Copper in Aqueous Electrolyte. *Chem. Rev.* **2019**, *119*, 7610–7672.

(2) Birdja, Y. Y.; Pérez-Gallent, E.; Figueiredo, M. C.; Göttle, A. J.; Calle-Vallejo, F.; Koper, M. T. M. Advances and Challenges in Understanding the Electrocatalytic Conversion of Carbon Dioxide to Fuels. *Nat. Energy* **2019**, *4*, 732–745.

(3) Gattrell, M.; Gupta, N.; Co, A. A Review of the Aqueous Electrochemical Reduction of CO_2 to Hydrocarbons at Copper. *J. Electroanal. Chem.* **2006**, *594*, 1–19.

(4) Kuhl, K. P.; Cave, E. R.; Abram, D. N.; Jaramillo, T. F. New Insights into the Electrochemical Reduction of Carbon Dioxide on Metallic Copper Surfaces. *Energy Environ. Sci.* **2012**, *5*, 7050–7059.

(5) Dinh, C.; Burdyny, T.; Kibria, G.; Seifitokaldani, A.; Christine, M. CO_2 Electroreduction to Ethylene via Hydroxide-Mediated Copper Catalysis at an Abrupt Interface. **2018**, *787*, 783–787.

(6) Zhang, B.; Zhang, J.; Hua, M.; Wan, Q.; Su, Z.; Tan, X.; Liu, L.; Zhang, F.; Chen, G.;

Tan, D.; Cheng, X.; Han, B.; Zheng, L.; Mo, G. Highly Electrocatalytic Ethylene Production from CO_2 on Nanodefective Cu Nanosheets. *J. Am. Chem. Soc.* **2020**, *142*, 13606–13613.

(7) Ting, L. R. L.; Piqué, O.; Lim, S. Y.; Tanhaei, M.; Calle-Vallejo, F.; Yeo, B. S. Enhancing CO_2 Electroreduction to Ethanol on Copper-Silver Composites by Opening an Alternative Catalytic Pathway. *ACS Catal.* **2020**, *10*, 4059–4069.

(8) Schouten, K. J. P.; Kwon, Y.; van der Ham, C. J. M.; Qin, Z.; Koper, M. T. M. A New Mechanism for the Selectivity to C_1 and C_2 Species in the Electrochemical Reduction of Carbon Dioxide on Copper Electrodes. *Chem. Sci.* **2011**, *2*, 1902–1909.

(9) Calle-Vallejo, F.; Koper, M. T. M. Theoretical Considerations on the Electroreduction of CO to C_2 Species on Cu(100) Electrodes. *Angew. Chemie Int. Ed.* **2013**, *52*, 7282–7285.

(10) Bertheussen, E.; Verdaguer-Casadevall, A.; Ravasio, D.; Montoya, J. H.; Trimarco, D. B.; Roy, C.; Meier, S.; Wendland, J.; Nørskov, J. K.; Stephens, I. E. L.; Chorkendorff, I. Acetaldehyde as an Intermediate in the Electroreduction of Carbon Monoxide to Ethanol on Oxide-Derived Copper. *Angew. Chemie Int. Ed.* **2016**, *55*, 1450–1454.

(11) Ledezma-Yanez, I.; Gallent, E. P.; Koper, M. T. M.; Calle-Vallejo, F. Structure-Sensitive Electroreduction of Acetaldehyde to Ethanol on Copper and Its Mechanistic Implications for CO and CO_2 Reduction. *Catal. Today* **2016**, *262*, 90–94.

(12) Hori, Y.; Takahashi, R.; Yoshinami, Y.; Murata, A. Electrochemical Reduction of CO at a Copper Electrode. *J. Phys. Chem. B* **1997**, *101*, 7075–7081.

(13) Ren, D.; Gao, J.; Pan, L.; Wang, Z.; Luo, J.; Zakeeruddin, S. M.; Hagfeldt, A.; Grätzel, M. Atomic Layer Deposition of ZnO on CuO Enables Selective and Efficient Electroreduction of Carbon Dioxide to Liquid Fuels. *Angew. Chemie* **2019**, *131*, 15178–15182.

(14) Li, F.; Li, Y. C.; Wang, Z.; Li, J.; Nam, D.-H.; Lum, Y.; Luo, M.; Wang, X.; Ozden, A.; Hung, S.-F.; Chen, B.; Wang, Y.; Wicks, J.; Xu, Y.; Li, Y.; Gabardo, C. M.; Dinh, C.-T.; Wang, Y.; Zhuang, T.-T.; Sinton, D.; Sargent, E. H. Cooperative CO_2-to-Ethanol Conversion via Enriched Intermediates at Molecule–Metal Catalyst Interfaces. *Nat. Catal.* **2020**, *3*, 75–82.

(15) Luo, W.; Nie, X.; Janik, M. J.; Asthagiri, A. Facet Dependence of CO_2 Reduction Paths on Cu Electrodes. *ACS Catal.* **2016**, *6*, 219–229.

(16) Bagger, A.; Ju, W.; Varela, A. S.; Strasser, P.; Rossmeisl, J. Electrochemical CO_2 Reduction: Classifying Cu Facets. *ACS Catal.* **2019**, *9*, 7894–7899.

(17) Karapinar, D.; Creissen, C. E.; Rivera De La Cruz, J. G.; Schreiber, M. W.; Fontecave, M. Electrochemical CO_2 Reduction to Ethanol with Copper-Based Catalysts. *ACS Energy Lett.* **2021**, *6*, 694–706.

(18) Todorova, T. K.; Schreiber, M. W.; Fontecave, M. Mechanistic Understanding of CO_2 Reduction Reaction (CO_2RR) Toward Multicarbon Products by Heterogeneous Copper-Based Catalysts. *ACS Catal.* **2020**, *10*, 1754–1768.

(19) Hori, Y.; Wakebe, H.; Tsukamoto, T.; Koga, O. Electrocatalytic Process of CO Selectivity in Electrochemical Reduction of CO_2 at Metal Electrodes in Aqueous Media. *Electrochim. Acta* **1994**, *39*, 1833–1839.

(20) Bagger, A.; Ju, W.; Varela, A. S.; Strasser, P.; Rossmeisl, J. Electrochemical CO_2 Reduction: A Classification Problem. *ChemPhysChem* **2017**, *18*, 3266–3273.

(21) Li, Y. C.; Wang, Z.; Yuan, T.; Nam, D.-H.; Luo, M.; Wicks, J.; Chen, B.; Li, J.; Li, F.; de Arquer, F. P. G.; Wang, Y.; Dinh, C.-T.; Voznyy, O.; Sinton, D.; Sargent, E. H. Binding Site Diversity Promotes CO_2 Electroreduction to Ethanol. *J. Am. Chem. Soc.* **2019**, *141*, 8584–8591.

(22) Morales-Guio, C. G.; Cave, E. R.; Nitopi, S. A.; Feaster, J. T.; Wang, L.; Kuhl, K. P.; Jackson, A.; Johnson, N. C.; Abram, D. N.; Hatsukade, T.; Hahn, C.; Jaramillo, T. F. Improved CO_2 Reduction Activity towards C_{2+} Alcohols on a Tandem Gold on Copper Electrocatalyst. *Nat. Catal.* **2018**, *1*, 764–771.

(23) Lum, Y.; Ager, J. W. Sequential Catalysis Controls Selectivity in Electrochemical CO_2 Reduction on Cu. *Energy Environ. Sci.* **2018**, *11*, 2935–2944.

(24) Chen, C.; Li, Y.; Yu, S.; Louisia, S.; Jin, J.; Li, M.; Ross, M. B.; Yang, P. Cu-Ag Tandem Catalysts for High-Rate CO_2 Electrolysis toward Multicarbons. *Joule* **2020**, *4*, 1688–1699.

(25) Iyengar, P.; Kolb, M. J.; Pankhurst, J. R.; Calle-Vallejo, F.; Buonsanti, R. Elucidating the Facet-Dependent Selectivity for CO_2 Electroreduction to Ethanol of Cu–Ag Tandem Catalysts. *ACS Catal.* **2021**, *11*, 4456–4463.

(26) Loiudice, A.; Lobaccaro, P.; Kamali, E. A.; Thao, T.; Huang, B. H.; Ager, J. W.; Buonsanti, R. Tailoring Copper Nanocrystals towards C_2 Products in Electrochemical CO_2 Reduction. *Angew. Chemie Int. Ed.* **2016**, *55*, 5789–5792.

(27) Huang, J.; Hörmann, N.; Oveisi, E.; Loiudice, A.; De Gregorio, G. L.; Andreussi, O.; Marzari, N.; Buonsanti, R. Potential-Induced Nanoclustering of Metallic Catalysts during Electrochemical CO_2 Reduction. *Nat. Commun.* **2018**, *9*, 3117.

(28) Mangione, G.; Huang, J.; Buonsanti, R.; Corminboeuf, C. Dual-Facet Mechanism in

Copper Nanocubes for Electrochemical CO_2 Reduction into Ethylene. *J. Phys. Chem. Lett.* **2019**, *10*, 4259–4265.

(29) Guidelli, R.; Compton, R. G.; Feliu, J. M.; Gileadi, E.; Lipkowski, J.; Schmickler, W.; Trasatti, S. Defining the Transfer Coefficient in Electrochemistry: An Assessment (IUPAC Technical Report). *Pure Appl. Chem.* **2014**, *86*, 245–258.

(30) Nie, X.; Esopi, M. R.; Janik, M. J.; Asthagiri, A. Selectivity of CO_2 Reduction on Copper Electrodes: The Role of the Kinetics of Elementary Steps. *Angew. Chemie - Int. Ed.* **2013**, *52*, 2459–2462.

(31) Rendón-Calle, A.; Low, Q. H.; Hong, S. H. L.; Builes, S.; Yeo, B. S.; Calle-Vallejo, F. How Symmetry Factors Cause Potential- and Facet-Dependent Pathway Shifts during CO_2 Reduction to CH_4 on Cu Electrodes. *Appl. Catal. B Environ.* **2021**, *285*, 119776.

(32) Hori, Y.; Takahashi, I.; Koga, O.; Hoshi, N. Electrochemical Reduction of Carbon Dioxide at Various Series of Copper Single Crystal Electrodes. *J. Mol. Catal. A Chem.* **2003**, *199*, 39–47.

(33) Kleis, J.; Greeley, J.; Romero, N. A.; Morozov, V. A.; Falsig, H.; Larsen, A. H.; Lu, J.; Mortensen, J. J.; Dułak, M.; Thygesen, K. S.; Nørskov, J. K.; Jacobsen, K. W. Finite Size Effects in Chemical Bonding: From Small Clusters to Solids. *Catal. Lett. 2011 1418* **2011**, *141*, 1067–1071.

(34) Tripković, V.; Cerri, I.; Bligaard, T.; Rossmeisl, J. The Influence of Particle Shape and Size on the Activity of Platinum Nanoparticles for Oxygen Reduction Reaction: A Density Functional Theory Study. *Catal. Lett. 2014 1443* **2014**, *144*, 380–388.

(35) Calle-Vallejo, F.; Martínez, J. I.; García-Lastra, J. M.; Sautet, P.; Loffreda, D. Fast Prediction of Adsorption Properties for Platinum Nanocatalysts with Generalized Coordination Numbers. *Angew. Chemie Int. Ed.* **2014**, *53*, 8316–8319.

(36) Iyengar, P.; Huang, J.; De Gregorio, G. L.; Gadiyar, C.; Buonsanti, R. Size Dependent Selectivity of Cu Nano-Octahedra Catalysts for the Electrochemical Reduction of CO_2 to CH4. *Chem. Commun.* **2019**, *55*, 8796–8799.

(37) Pankhurst, J. R.; Guntern, Y. T.; Mensi, M.; Buonsanti, R. Molecular Tunability of Surface-Functionalized Metal Nanocrystals for Selective Electrochemical CO_2 Reduction. *Chem. Sci.* **2019**, *10*, 10356–10365.

(38) De Gregorio, G. L.; Burdyny, T.; Loiudice, A.; Iyengar, P.; Smith, W. A.; Buonsanti, R. Facet-Dependent Selectivity of Cu Catalysts in Electrochemical CO_2 Reduction at Commercially Viable Current Densities. *ACS Catal.* **2020**, *10*, 4854–4862.

(39) Schreier, M.; Yoon, Y.; Jackson, M. N.; Surendranath, Y. Competition between H and

CO for Active Sites Governs Copper-Mediated Electrosynthesis of Hydrocarbon Fuels. *Angew. Chemie Int. Ed.* **2018**, *57*, 10221–10225.

(40) Li, Y. C.; Wang, Z.; Yuan, T.; Nam, D.-H.; Luo, M.; Wicks, J.; Chen, B.; Li, J.; Li, F.; de Arquer, F. P. G.; Wang, Y.; Dinh, C.-T.; Voznyy, O.; Sinton, D.; Sargent, E. H. Binding Site Diversity Promotes CO_2 Electroreduction to Ethanol. *J. Am. Chem. Soc.* **2019**, *141*, 8584–8591.